ELSEVIER

Thermochimica Acta 391 (2002) 219–225

thermochimica acta

www.elsevier.com/locate/tca

Temperature modulated DSC for the multiple glass transition in poly(*n*-alkyl methacrylates)

E. Hempel*, M. Beiner, H. Huth, E. Donth

Fachbereich Physik, Universität Halle, 06099 Halle, Germany

Received 10 September 2001; accepted 6 November 2001

Abstract

Dielectric and mechanical relaxation processes in the series of poly(*n*-alkyl methacrylates) (P*n*AMA) depend systematically on the number of carbons in the alkyl part of the side chain. The crossover region of the dynamic glass transition shifts to lower frequencies for increasing this C number and reaches, above the hexyl member ($C = 6$), frequencies accessible to the temperature modulated DSC (TMDSC). The whole series from $C = 1$ (poly(methyl methacrylate), PMMA) to $C = 11$, the undecyl member is investigated by TMDSC and enthalpy retardation with DSC. The calorimetric result in the series are compared with the dielectric and mechanical data and are discussed with respect to the crossover region and a polyethylene-like glass transition (α_{PE} process) due to a nanophase separation in these homopolymers.

Keywords: Multiple glass transition; Poly(*n*-alkyl methacrylates); Temperature modulated DSC; Crossover; Nanophase separation

1. Introduction

Dielectric and mechanical measurements show that the relaxation spectrum of the poly(*n*-alkyl methacrylates) (P*n*AMA) includes several relaxation processes whose frequency–temperature position depends systematically on the C number of carbon atoms in the alkyl part of the side chain. The crossover region of the dynamic glass transition shifts towards lower frequencies and temperatures with increasing C number [1]. For the higher members of this homologous series an additional α_{PE} process within a nanophase of aggregated alkyl side chains was observed [2].

The crossover region of the dynamic glass transition is explained in the Arrhenius diagram (Fig. 1A). For high frequencies and temperatures we have the high-temperature process '**a**' that is described by the mode coupling theory. For low frequencies and temperatures, below the crossover region '**C**', we have two processes: the cooperative α process and the local β (Johari Goldstein) process. The thermal glass transition is observed if the α process frequency reaches about $\omega \approx 10^{-2}\,\mathrm{rad\,s^{-1}}$, this defines the glass temperature T_g usually well below the crossover temperature, T_c.

The Arrhenius diagram of Fig. 1A shows schematically the frequency dependence for a P*n*AMA with a given C number. Consider now a given frequency (e.g. $\omega = 10\,\mathrm{rad\,s^{-1}}$) and the dependence on the C number, i.e. changes along the P*n*AMA series. Since the crossover shifts systematically, we get a map of the Arrhenius diagram with given C number in the $T_{relax}-C$ number diagram for given frequency ω (Fig. 1B, [2]). The crossover region has the same topology in both diagrams. Additionally, we observe the α_{PE} process due to a nanophase separation. The alkyl parts are, in a

* Corresponding author. Fax: +49-345-55-27017.
E-mail address: e.hempel@physik.uni-halle.de (E. Hempel).

0040-6031/02/$ – see front matter
PII: S0040-6031(02)00185-5

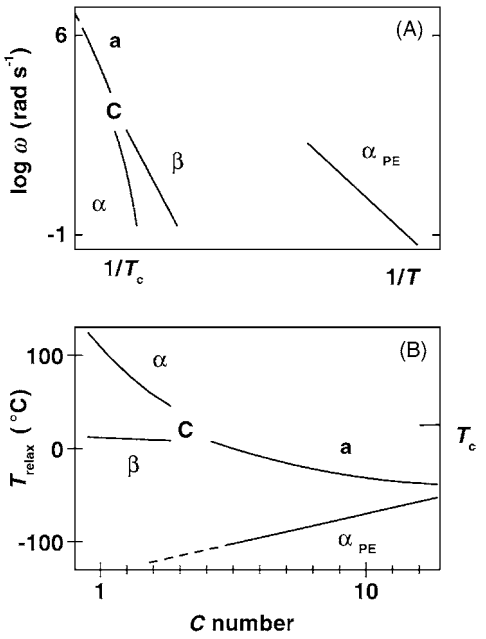

Fig. 1. Multiplicity of dynamic glass transition in the P*n*AMA series. (A) Arrhenius diagram for a given substance (given C number). (B) Relaxation temperature T_{relax} as a function of C number (different substances) for $\omega = 10\ rad\ s^{-1}$ from shear measurements (schematically from [2]). The processes are explained in the text.

way, incompatible with the neighboring main chain parts. Large phase regions, however, are excluded because of the chemical bonding between the alkyl groups and the main chains.

The crossover region in several P*n*AMA members $C \leq 8$ are studied in detail in [1,3–5]. The relaxation behavior of some higher members ($C = 10$ and 12) are investigated by Floudas and coworkers with photon correlation spectroscopy and other methods [6] and are compared with that of the lower members.

The aim of this paper is to investigate the calorimetric activity of the P*n*AMA relaxation processes as far as they are in the small frequency window below $\omega \approx 0.1\ rad\ s^{-1}$ accessible by temperature modulated DSC (TMDSC) and DSC (enthalpy retardation). A special problem is the separation of the '**a**' and α_{PE} processes for the higher C members.

2. Experimental

The P*n*AMA were synthesized by standard free-radical polymerization except the octyl and nonyl samples, which are prepared by living polymerization. All samples have high molecular weight ($M_w > 10^5\ g\ mol^{-1}$) and similar tacticity (ca. 78% syndiotactic diades); i.e. the relative temperature shift of the glass temperature due to tacticity or molecular weight are negligible. Table 1 gives a summary of the used P*n*AMA. The sample mass for DSC measurements was about 10 mg. A DSC 7 instrument (Perkin-Elmer) with TMDSC software option was used. The DSC was calibrated at zero heating rate according to the GEFTA recommendation [8]. The calibration was checked in the TMDSC

Table 1
Calorimetric parameters for P*n*AMA[a]

C numbers	Abbreviation	Full name	$T_{half\ step}$ (°C), $t_p = 60$ s	T_{peak} (°C), $t_p = 60$ s
1	PMMA	Poly(methyl methacrylate)	109	110.8
2	PEMA	Poly(ethyl methacrylate)	75	78.4
3	P*n*PrMA	Poly(*n*-propyl methacrylate)	58	60.7
4	P*n*BMA	Poly(*n*-butyl methacrylate)	30	33.9
5	P*n*PenMA	Poly(*n*-pentyl methacrylate)	12	15.4
6	P*n*HMA	Poly(*n*-hexyl methacrylate)	−10	−2
7	P*n*HepMA	Poly(*n*-heptyl methacrylate)	−15	−10
8	P*n*OMA	Poly(*n*-octyl methacrylate)	−30	−24
9	P*n*NMA	Poly(*n*-nonyl methacrylate)	−31	−25
10	P*n*DMA	Poly(*n*-decyl methacrylate)	−45	−57, −27
11	P*n*UMA	Poly(*n*-undecyl methacrylate)	−59	−48

[a] $T_{half\ step}$-half step temperature from c_p' (error: ±1 K for $C = 1, \ldots, 5$ and ±2 K for $C = 6, \ldots, 11$) and T_{peak}-maximum temperature from a Gaussian fit for c_p'' (error: ±0.5 K for $C = 1, \ldots, 5$ and ±2 K for $C = 6, \ldots, 11$). The determination of the glass temperature T_g from an equal-area construction according to Richardson and Savill [7] was impossible due to problems with accurate C_p-measurements at low temperature in the specific case of the P*n*AMA series.

mode with the smectic A to nematic transition of the liquid crystal 8OCB [9,10]. Nitrogen gas with a flow rate of about 20 ml min^{-1} was purged through the cell. For measurements on P*n*AMA with $C > 5$ liquid nitrogen was used for cooling. TMDSC measurements are performed with sawtooth-like modulation (t_p = 60 s, $T_a = 0.3$ K) and an underlying cooling rate ($q = 0.5$ K min^{-1}). Data evaluation methods are described in [11].

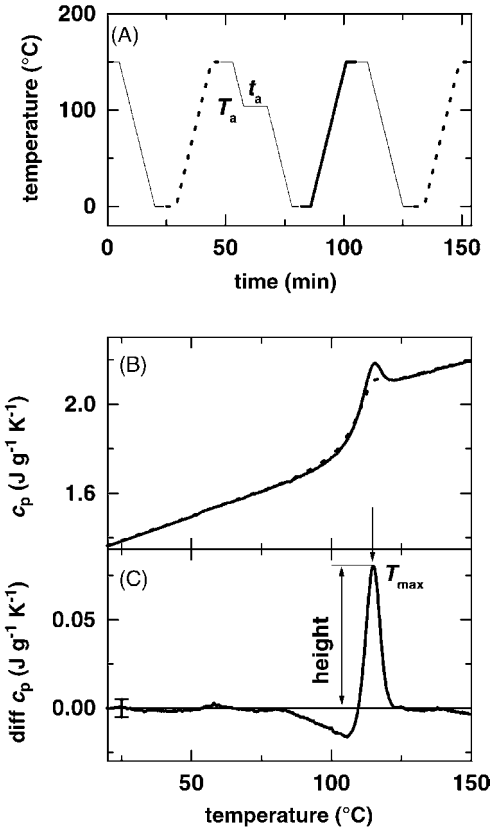

Fig. 2. (A) Temperature–time program for the enthalpy retardation experiment. Heating and cooling rates are always identical: $|dT/dt| = 10$ K min^{-1} for P*n*AMA with $1 \le C \le 4$ and $|dT/dt| = 20$ K min^{-1} for $C \ge 5$, respectively. The solid line represents the heating run after an annealing time $t_a = 10$ min at the annealing temperature T_a and dotted lines represent heating runs without prior isothermal annealing. (B) Specific heat c_p from heating runs for PMMA. The solid line represents a DSC scan with annealing and the dotted line represents a DSC scan without annealing. (C) Difference between the c_p curves with and without annealing. The curves were calculated directly from the heat flow curves without using measurements with empty sample pan. The peak is described by the maximum temperature T_{max} and the peak height. The error bar indicates the uncertainty ($\delta c_p = \pm 0.005$ J g^{-1} K^{-1}).

The enthalpy retardation program for the additional DSC enthalpy retardation experiments is shown in Fig. 2A. A typical result of an enthalpy retardation experiment with an annealing time $t_a = 10$ min at an annealing temperature $T_a = 104$ °C is presented for poly(methyl methacrylate) (PMMA) in Fig. 2B and C. The difference curve is a relaxation peak characterized by the peak height at the temperature T_{max}.

A Novocontrol setup with a Schlumberger SI 1260 response analyzer was used for dielectric measurements. The dielectric function $\varepsilon^* = \varepsilon' - i\varepsilon''$ was measured in a frequency range from 10^{-2} to 10^6 Hz. The samples were equilibrated at each temperature for about 600 s before the isothermal frequency sweep was started. The effective "cooling rate" was about 0.2 K min^{-1}, the temperature step was usually 5 K. One or a sum of two Havriliak Negami (HN) functions [12]

$$\varepsilon^* = \varepsilon'(\omega) - i\varepsilon''(\omega) = \Delta\varepsilon\left(1 + \left(\frac{i\omega}{\omega_c}\right)^b\right)^{-g} + \varepsilon_\infty,$$

and if necessary an additional conductivity term ($\sigma \sim \omega^{-1}$), were used to fit the isothermal ε^* data (for details, see [1,16]). The RDA II rheometer (Rheometrics) was used to measure the temperature and frequency dependence of the shear modulus $G^* = G' + iG''$. The sample geometry was a strip of about 1.5 mm × 10 mm × 25 mm. The samples were equilibrated at each temperature for 100 s prior to the isothermal measurements at 0.1, 1, 10, and 100 rad s^{-1}. The effective cooling rate was about 0.5 K min^{-1}, the temperature step was 3 K.

3. Results

The results of the TMDSC measurements for a series of P*n*AMA are shown in Fig. 3. The typical glass step in the real part of the dynamic heat capacity c_p' and the peak maximum in the imaginary part c_p'' are shifted to lower temperature with increasing C number of the alkyl side chain. The half step temperatures from c_p' and the maxima temperatures from Gaussian fits to c_p'' curves are listed in Table 1. While for a conventional glass transition both temperatures are

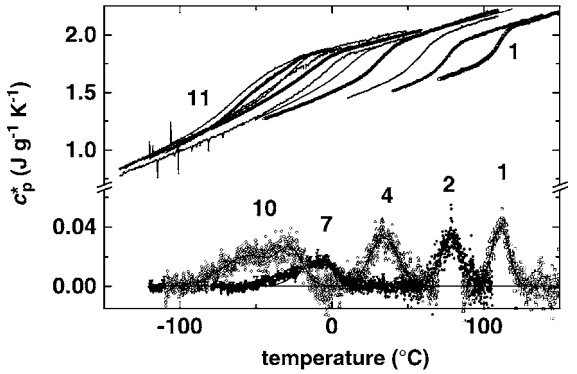

Fig. 3. Real and imaginary parts of the complex heat capacity $c_p^* = c_p' - ic_p''$ from TMDSC (time period $t_p = 60$ s, underlying cooling rate 0.5 K min^{-1}) for P*n*AMA from $C = 1$ to 11. For reasons of clarity, the imaginary parts are only given for $C = 1$ (□), 2 (●), 4 (△), 7 (▼), and 10 (◇).

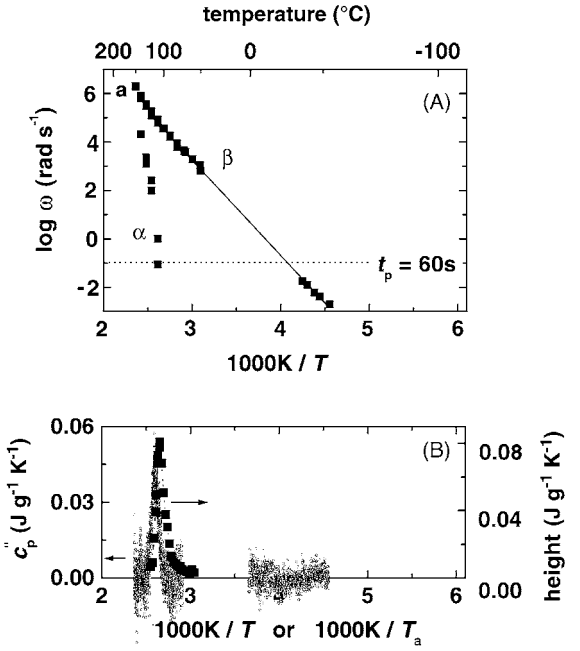

Fig. 4. Results from dielectrics and calorimetry for PMMA. (A) Arrhenius diagram with ε'' peak frequencies from dielectrics. The log ω value for TMDSC measurements with $t_p = 60$ s is indicated by the dotted line. Dielectric data at low frequencies are from [13]. The labels indicate the different relaxation processes. (B) Results from calorimetry: imaginary part c_p'' from TMDSC (○) and response from the enthalpy retardation experiment (■) vs. reciprocal temperature.

usually identical [18], there is a difference between both temperatures for our P*n*AMA. The temperature difference systematically increases from 2 to 10 K with increasing side chain length. Moreover, the imaginary peak becomes broader and asymmetrical at low temperatures. The peak height dramatically decreases from about 0.04 J g^{-1} K^{-1} for PMMA down to small values of about 0.02 J g^{-1} K^{-1} for poly(*n*-heptyl methacrylate) (P*n*HepMA) which is only three times larger than the noise (±0.007 J g^{-1} K^{-1}) under the given experimental conditions. The weakly structured broad glass transitions for higher P*n*AMA ($C > 6$) do not allow to separate different contributions. For poly(*n*-decyl methacrylate) ($C = 10$) there are indications for at least two coexisting processes, one at a temperature near −25 °C and another one at temperatures near −60 °C [2]. In order to clarify the reasons for the peak broadening with increasing side chain length, the imaginary part c_p'' is compared with the results from dielectric (ε'') and shear measurements (G'') at a comparable frequency. Isochrones and Arrhenius plot for three P*n*AMA will be presented in the following in order to visualize the relation between the three different glass transitions in this series of side chain polymers.

TMDSC measurements for PMMA at a frequency of $\log(\omega/\text{rad s}^{-1}) = -1$ detect the conventional α process clearly below the crossover region which is found in dielectric data in the megahertz range (Fig. 4A). A symmetric and narrow $c_p''(T)$ peak is observed. The enthalpy retardation experiment for PMMA gives a peak with similar width (ca. 12 K) at slightly lower temperatures (Fig. 4B). TMDSC measurements in the temperature region of the β process show no significant calorimetric signal in $c_p''(T)$ (Fig. 4B), i.e. the β process is not, or only slightly calorimetrically active, as usual [14,15].

The crossover region for P*n*HepMA is shifted to lower frequency in the Arrhenius plot (Fig. 5A). The dielectric results show the crossover region at $\log(\omega/\text{rad s}^{-1}) = 0$ slightly above the TMDSC frequency. The $c_p''(T)$ peak from TMDSC is broad with a peak maximum near the α process and asymmetric with a low temperature tail (Fig. 5B). The calorimetry probably detects the α process and additional contributions from the dying '**a**' process at slightly lower temperatures. Indications for such a dying, less activated '**a**' process are found in the crossover region of poly(*n*-hexyl methacrylate) (P*n*HMA) using the 3ω

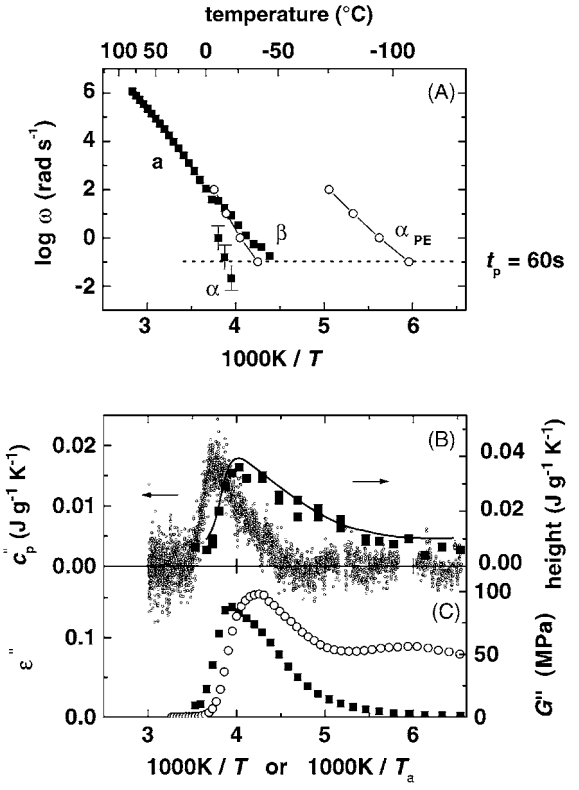

Fig. 5. Results from dielectrics, shear, and calorimetry for P*n*HepMA. (A) Arrhenius diagram with dielectric (■) and shear results (○), $\log \omega$ for TMDSC with $t_p = 60$ s is indicated. (B) Results from calorimetry: imaginary part c_p'' from TMDSC (○) and response from the enthalpy retardation experiment (■). The measured phase angle is disturbed by losing the contact between sample and pan at temperatures $T = -106$ °C and -80 °C. This was corrected by a vertical shift. (C) Loss part of dielectric function (■) and shear loss modulus (○) as function of reciprocal temperature. Frequency is 0.1 rad s^{-1} $\log(\omega/\text{rad s}^{-1}) = -1$ for both curves similar to TMDSC frequency $\omega_p = 2\pi/t_p = 2\pi/60$ s $\log(\omega/\text{rad s}^{-1}) = 0.98$. Details of the time–temperature program are given in Section 2.

method of heat capacity spectroscopy [4]. Note, that there are differences between ε'', G'', and $c_p''(T)$ in Fig. 5 due to the fact that each susceptibility reflects a specific fluctuation. Therefore, the frequency temperature position of dynamic glass transition is slightly activity-dependent and different relaxation processes are more or less intense for different susceptibilities [16,17]. An additional α_{PE} glass transition near -100 °C is found in shear measurements for P*n*HepMA (Fig. 5C). This "polyethylene-like" glass transition is not active in dielectrics because it occurs in aggregated alkyl rests without significant dipole moment [2]. In TMDSC data for P*n*HepMA the α_{PE} glass transition could not be detected. In the TMDSC cooling experiment, the measurement at low temperatures is disturbed by effects caused by loosing the contact between the sample and the pan. There are no significant $c_p''(T)$ signals above the noise level near -100 °C for P*n*HepMA. Obviously, the calorimetric intensity of the α_{PE} process is too small to be detected by TMDSC. It is not easy to measure accurate phase angles in TMDSC scans over a wide temperature range of about 200 K including temperatures down to -100 °C. The enthalpy retardation experiments, however, show a pronounced low temperature tail with

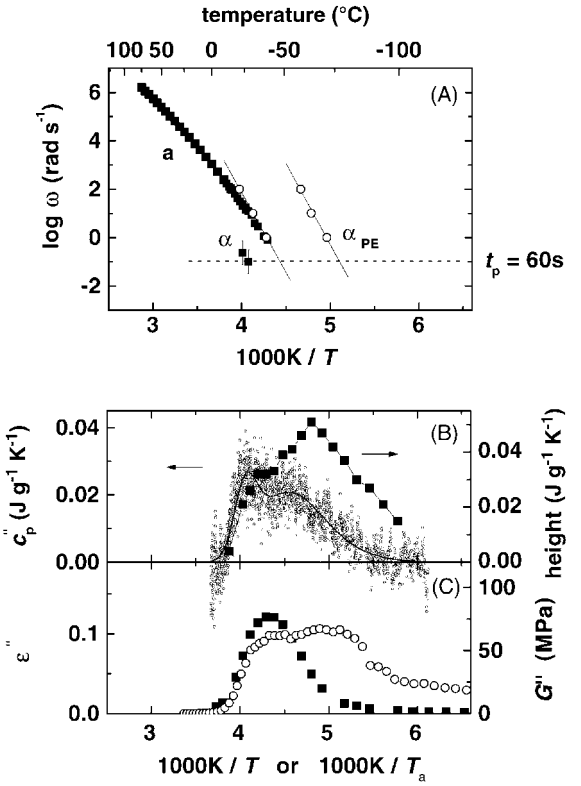

Fig. 6. Results from dielectrics, shear, and calorimetry for P*n*DMA. (A) Arrhenius diagram with dielectric (■) and shear results (○), $\log \omega$ for TMDSC with $t_p = 60$ s is indicated. (B) Results from calorimetry: imaginary part c_p'' from TMDSC (○) and response from enthalpy retardation experiment (■). (C) Loss part of dielectric function (■) at a frequency of 0.1 rad s^{-1} $\log(\omega/\text{rad s}^{-1}) = -1$ and shear loss modulus (○) at 1 rad s^{-1} $\log(\omega/\text{rad s}^{-1}) = 0$ vs. reciprocal temperature.

significant contributions ($\Delta c_p \geq 0.005\ \mathrm{J\ g^{-1}\ K^{-1}}$) in the temperatures range of the α_{PE} glass transition near $T \approx -100\ ^\circ\mathrm{C}$.

For poly(*n*-decyl methacrylate) (P*n*DMA) the crossover frequency is still lower than that of P*n*HepMA, and very close to the TMDSC frequency of $\log(\omega/\mathrm{rad\ s^{-1}}) = -1$ (Fig. 6A). In addition the difference between α and α_{PE} glass transition ($T_{g,\alpha} - T_{g,\alpha_{PE}} \approx 50\ \mathrm{K}$) is smaller compared to those for P*n*HepMA (≈85 K). The $c_p''(T)$ peak and the enthalpy retardation experiments for P*n*DMA show both a double peak structure with a slightly different intensity ratio (Fig. 6B). Obviously, calorimetric data reflect the main transition (α, '**a**') in the crossover region and additional contributions of the α_{PE} glass transition at lower temperatures. In enthalpy retardation experiments a response is found still below $-80\ ^\circ\mathrm{C}$ with $\Delta c_p \geq 0.010\ \mathrm{J\ g^{-1}\ K^{-1}}$. This is twice the uncertainty ($\delta c_p \approx \pm 0.005\ \mathrm{J\ g^{-1}\ K^{-1}}$) of our measurements. The existence of the $c_p''(T)$ peak (and the enthalpy response) in the low temperature region results from the more pronounced α_{PE} process in P*n*DMA consistent with the large volume fraction of alkyl side chains in this polymer. An intense α_{PE} process is also observed in shear data for P*n*DMA. Again, the α_{PE} process is practically not active in dielectric response (Fig. 6C), since the alkyl nanodomains do not contain significant dipole moments from main chain segments.

4. Discussion

There are two main effects which are important for an understanding of the changes in TMDSC curves with side chain length for P*n*AMA. (i) The crossover frequency approaches the TMDSC frequency with increasing side chain length. TMDSC detects the superposition of contributions from '**a**' and α processes near the crossover region in the higher members ($6 < C \leq 11$). The glass temperature of the main transition (α,'**a**') process shifts systematically to lower temperatures due to internal plasticization. (ii) We have a systematic increase of the volume fraction of the alkyl nanodomains and a more intense α_{PE} process with increasing number of the alkyl carbons (C number) in the side chain. Thus, there are increasing contributions to $c_p''(T)$ in TMDSC data at low temperatures. By the way, this influences the accuracy of the tangents in the glassy state and finally the determination of the half step temperature from $c_p'(T)$.

We conclude from the comparison of different susceptibilities (Figs. 4–6) that it is not easy to measure the α_{PE} glass transition for P*n*AMA by TMDSC. For the lower P*n*AMA with $C < 8$ the intensity of the '**a**' (or α) process is much larger than that for the α_{PE} process. This is due to the small volume content of the alkyl nanodomains and to the large distance between α and α_{PE} glass transitions. It is difficult to measure such a small $c_p''(T)$ contribution over an huge temperature range. For the higher P*n*AMA ($C = 10$ and 11) we have a significant α_{PE} intensity, but the distance between α and α_{PE} glass transitions is small and the TMDSC frequency is near the crossover frequency. Consequently, it is difficult to separate the α_{PE} glass transition from the broad (α, '**a**') peak for those members. The α, '**a**' and the α_{PE} contributions do overlap. Dynamic heat capacity reflects the complicated superposition of contributions from the three different glass transitions ('**a**', α, α_{PE}) in these polymers.

We obtained comparable results from TMDSC and enthalpy retardation experiments for all P*n*AMA. In detail, there are differences at low temperatures caused by the α_{PE} glass transition. This may result from different reasons, e.g. aging effects during the annealing time, possible changes in the morphology with temperature, or a stabilization or amplification of the nanophase separation of incompatible main and side chain parts resulting in a perfection of the phase separation. Moreover, there may be changes in the side chain order with annealing time and with side chain length for P*n*AMA.

Because of the above discussed problems with accurate measurements of the phase angle for lower C numbers we are able to detect the α_{PE} glass transition by TMDSC only for $C = 10$ and 11. For the members of the P*n*AMA series with $C \geq 4$, however, we have definite indications for a calorimetric response in enthalpy retardation experiments at low temperatures indicating the α_{PE} glass transition.

5. Conclusions

The calorimetric activity of the '**a**' and α processes in the P*n*AMA series corresponds to their dielectric

and mechanical activities. The α_{PE} process (active in mechanical and practically non-active in dielectric measurements) is difficult to detect by TMDSC, especially in the phase shift necessary for the determination of the imaginary part of heat capacity. The main problem is to hold the TMDSC regime stable over such large temperature regions needed to detect two broad and overlapping peaks as for the '**a**' and α_{PE} processes and to separate the different contributions. Parallel enthalpy retardation investigations from DSC gave, however, clear indications for the calorimetric activity of the two processes for the higher P*n*AMA. There are different details in the TMDSC and enthalpy retardation that could be explained by the completion of the nanophase separation during the enthalpy retardation experiments by DSC.

Acknowledgements

We thank Dr. S. Reissig for providing dielectric data for PMMA. Financial support by the Deutsche Forschungsgemeinschaft DFG (SFB 418) is acknowledged.

References

[1] F. Garwe, A. Schönhals, H. Lockwenz, M. Beiner, K. Schröter, E. Donth, Macromolecules 29 (1996) 247.
[2] M. Beiner, K. Schröter, E. Hempel, S. Reissig, E. Donth, Macromolecules 32 (1999) 6278.
[3] K. Schröter, R. Unger, S. Reissig, F. Garwe, S. Kahle, M. Beiner, E. Donth, Macromolecules 31 (1998) 8966.
[4] M. Beiner, S. Kahle, E. Hempel, K. Schröter, E. Donth, Europhys. Lett. 44 (1998) 321;
M. Beiner, S. Kahle, E. Hempel, K. Schröter, E. Donth, Macromolecules 31 (1998) 8973.
[5] R. Bergman, F. Alvarez, A. Alegria, J. Colmenero, J. Chem. Phys. 109 (1998) 7546;
R. Bergman, F. Alvarez, A. Alegria, J. Colmenero, J. Non-Cryst. Solids 235–237 (1998) 580.
[6] G. Floudas, P. Placke, P. Stepanek, W. Brown, G. Fytas, K.L. Ngai, Macromolecules 28 (1995) 6799;
G. Floudas, P. Stepanek, Macromolecules 31 (1998) 6951.
[7] M.J. Richardson, N.G. Savill, Polymer 16 (1975) 753.
[8] S.M. Sarge, W. Hemminger, E. Gmelin, G.W.H. Höhne, H.K. Cammenga, W. Eysel, J. Thermal Anal. 49 (1997) 1125.
[9] A. Hensel, C. Schick, Thermochim. Acta 304–305 (1997) 229.
[10] C. Schick, U. Jonsson, T. Vassiliev, A. Minakov, J. Schawe, R. Scherrenberg, D. Lörinczy, Thermochim. Acta 347 (2000) 53.
[11] S. Weyer, A. Hensel, C. Schick, Thermochim. Acta 304–305 (1997) 267.
[12] S. Havriliak, S. Negami, J. Polym. Sci.: Part C 14 (1966) 99.
[13] S. Reissig, Ph.D. Thesis, Universität Halle, Halle, 1999.
[14] S.S.N. Murthy, Gangasharan, S.K. Nayak, J. Chem. Soc., Faraday Trans. 89 (1993) 509
[15] K. Kishimoto, H. Suga, S. Seki, Bull. Chem. Soc. Jpn. 46 (1973) 3020.
[16] M. Beiner, O, Kabisch, S. Reichl, H. Huth, J. Non-Cryst. Solids (2002), in press.
[17] M. Beiner, J. Korus, H. Lockwenz, K. Schröter, E. Donth, Macromolecules 29 (1996) 5183.
[18] A. Hensel, Ph.D. Thesis, Universität Rostock, 1998, p. 59.